TENSORIAL EQUATIONS FOR THREE-DIMENSIONAL LAMINAR BOUNDARY LAYER FLOWS

Mario A. Storti, Jorge D'Elía and Laura Battaglia

Centro Internacional de Métodos Computacionales en Ingeniería (CIMEC), Instituto de Desarrollo Tecnológico para la Industria Química (INTEC), Universidad Nacional del Litoral - CONICET , Güemes 3450, 3000-Santa Fe, Argentina, e-mail: mstorti@intec.unl.edu.ar, jdelia@intec.unl.edu.ar, lbattaglia@santafe-conicet.gov.ar, web page: http://www.cimec.org.ar

Keywords: three-dimensional surfaces, Christoffel symbols, tensor analysis, boundary-layer laminar flows, incompressible viscous fluid, fluid mechanics

Abstract. Tensorial equations are derived for a laminar and attached boundary layer flow with null pressure gradient in the direction normal to a smooth three-dimensional surface. An incompressible, isothermal and viscous fluid of Newtonian type is assumed. Covariant derivatives in the three dimensional Euclidean domain are employed, where the surface curvature terms are implicitly included in the related Christoffel symbols with the aim of writing the boundary layer equations in an invariant form irrespective to the particular choice of the coordinate system. These equations are covariant under a linear coordinate transformation on the two surface coordinates, and a scaling along the direction normal to the body surface one. As a test case, the boundary layer near a sphere in an axisymmetrical steady flow is numerically computed using a pseudo-spectral approach.

1 INTRODUCTION

As it is well known, mechanical devices may require the calculation of fully three-dimensional boundary layersSchlitchting and Gersten (2004), as those associated with flow inside turbomachines Lakshminarayana (1995), horizontal-axis wind turbine blades Prado (1995), laminar flow technology Stock (2006) or aerospace technology Dwoyer et al. (1978), among other cases. The laminar boundary layer equations for three-dimensional surfaces are well known and were derived by Howarth (1951) in a general orthogonal coordinate system and by Squire (1957) in a restricted nonorthogonal case. In any case, there are curvature effects that do not disappear as they do in the two-dimensional case Reed and Lin (1993). In fact, in the Howard's derivation, these are present through the principal curvatures of the surface. If one of them is null the boundary layer equations are independent of the curvature effects, as in planes, yawed infinite cylinders or wings Pai (1956).

As it is known, there is nothing special about a particular system of surface coordinates, so the physics behind the equations for the boundary layer flow should be independent of them. Nevertheless, Kaplun (1954) has shown in the case of steady, two-dimensional, incompressible and attached flow, that the approximate solution given by the boundary layer theory depends on the system of coordinates used when simplifying assumptions are applied to the Navier–Stokes equations so, in general, different systems of coordinates lead to boundary layer equations which are not fully equivalent and their solutions represent different flow fields, that is, they are not covariants. For instance, Kaplun considered the case of the boundary layer solutions for flow past a semi-infinite flat plate when rectangular or parabolic coordinates are used, and found that a boundary layer solution with respect to any given system can be found by substitution. Besides, it was also shown that the skin friction is invariant but the flow field is not, in the sense that the flow field given by the boundary layer theory at large distances from the wall depends almost entirely on the choice of the coordinates rather than on the physical problem.

In other way, Panaras (1987) gave the formulation of the unsteady, compressible Navier–Stokes covariant equations in general non-orthogonal curvilinear coordinates and thereafter a discussion follows about the terms which could be omitted in a thin shear-layer formulation, while the present work considers steady, incompressible fluid flow using covariant derivative in an orthogonal coordinate system but it is not a special case. The main differences are: (i) Panaras wrote the boundary layer equations in a full way with several surface curvature terms explicitly given, while here, they are implicitly included in the Christoffel symbols of the covariant derivatives with the main aim of putting the boundary layer equations in invariant form irrespective to the particular choice of the coordinate system, and (ii) a slight difference exists in the choice of the coordinate normal to the surface. As it is well known in standard boundary-layer engineering, the surface curvature terms (i.e. the normal pressure gradient) are the first terms to be added when Prandtl basic equations are extended to the three dimensional case and there are many expressions proposed in literature, partially due to the several approximations that can be performed with the curvature terms. But a rather shortcoming of many of them is that a detailed check about its physical invariance is frequently cumbersome to perform. Therefore, in order to obtain a more physical picture and an easier verification, it would convenient placing the surface curvature terms only in the covariant derivatives rather than displayed in the boundary layer equations.

On the other hand, a full numerical solution of the Navier–Stokes equations for high Reynolds numbers is nowadays a standard approach, like those based in the Reynolds Averaged Navier–Stokes (RANS) equations (see for example Wilcox, 1998), Large Eddy Simulations (LES) (see

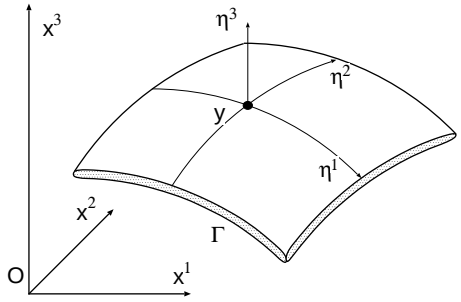

Figure 1: Dimensionless coordinates: surface intrinsic (η^1, η^2) on the smooth surface Γ, the normal coordinate η^3 and the point $\mathbf{y} = (y^1, y^2, y^3) \in \Gamma$ in the three-dimensional Cartesian space $\mathbb{R}^3$.

for example Sagaut, 2001) and Direct Numerical Simulations (DNS) (see for example Pope, 2003), among several approaches. Nevertheless, three-dimensional boundary layers and boundary layer separation are still areas where boundary layer computations may deserve as a complementary tool (see for example Cebeci and Cousteix, 1999; Dey, 2001), for instance, coupled viscous-inviscid computations for wind turbine airfoil flows Bermúdez et al. (2002), unsteady flows in turbomachinery Epureanu et al. (2001), unsteady interaction with outer transonic flows Bogdanov and Diyesperov (2005), flows past moving bands Frondelius et al. (2006), as well as oscillatory boundary layers attached to deformable solid walls using matched asymptotic expansions Nicols and Vega (2003). They are also proposed as alternatives to the classical convective outlet boundary condition heavily used for wall-bounded laminar/turbulent flows Fournier et al. (2008). In fact, three-dimensional boundary layer methods are likely to be both more accurate and less computationally expensive than a full numerical solution of the Navier–Stokes equations and they can be performed using classical approaches, as the integral ones used in Karimipanah and Olsson (1993), where the effects of rotation and compressibility on rotor blade boundary layers are studied, or a somewhat more modern resources as finite differences Anderson (1985), finite elements Schetz (1991) and pseudo-spectral approaches Storti (1998). In any case, their solutions can be used for testing more elaborated computational codes as those that directly solve the Navier–Stokes equations in several contexts, for instance, with the PETSc-FEM (2008) code used for modeling free surface flows D'Elía et al. (2000); Battaglia et al. (2006), added mass computations Storti and D'Elía (2004) or inertial waves in closed flow domains D'Elía et al. (2006).

The present work develops a covariant derivation of the boundary layer equations in tensorial form valid for three-dimensional, steady and laminar boundary layers with null-pressure gradient in the direction normal to the body surface. They are written in an orthogonal curvilinear coordinate system, defined by two surface coordinates plus a normal one to the surface, such that: (i) they are covariant under a coordinate transformation on the two intrinsic surface coordinates and a scaling one along the normal coordinate to the body surface; (ii) the surface curvature terms are implicitly present in the covariant derivatives and not in the displayed equations in opposite case to the more traditional way that typically include the surface curvature, surface principal curvatures or related terms in the boundary layer equations; (iii) there only remains the surface metric tensor in the continuity equation. As a practical use of the proposed covariant formalism, the steady and laminar three-dimensional boundary layer flow near a moving sphere of an incompressible and viscous fluid is performed as a test case using a pseudo-spectral approach, first without a rotation and later with a steady spin rotation.

2 SURFACE AND EXTENDED COORDINATES

In all this work, Latin affixes run in the three-dimensional Cartesian space, e.g. $i = 1, 2, 3$, the Greek ones run on the two-dimensional surface, e.g. $\alpha = 1, 2$, while upper and lower affixes denote contravariant and covariant components of tensors of any range (see for example Smith, 1963; Aris, 1989). Lower and upper Roman letters denote dimensionless and dimension quantities, respectively. The basic ones are the coordinates $x^i = X^i/L$, velocities $u^i = U^i/U$ and pressure $p = P/(\rho U^2)$, where U, L and ρ are typical speed, length and fluid density, respectively, while, regarding incompressibility of the fluid, the fluid density ρ is constant.

It is assumed that the body surface $\mathit{\Gamma}$ is smooth enough to be represented by a coordinate grid on the surface itself, expressing the position of a surface point in terms of the dimensionless surface coordinates. Thus, the surface equation has the form $x^i = x^i(\eta^1, \eta^2)$, where η^1, η^2 are the surface coordinates, the intrinsic ones, while the lines $\eta^1 =$ constant and $\eta^2 =$ constant are the coordinate lines. The Cartesian coordinates $\boldsymbol{y} = (y^1, y^2, y^3)^T \in \mathbb{R}^{3\times 1}$, for a generic point $\boldsymbol{y}$ on the surface $\mathit{\Gamma}$ can be expressed as a function of the surface coordinates $\boldsymbol{y} = \boldsymbol{y}(\eta^1, \eta^2)$, see figure 1, where $(...)^T$ denotes the transpose. An extended coordinate system (η^1, η^2, η^3) is introduced as a three-dimensional curvilinear one for extending the surface coordinates to the three-dimensional space where the body is immersed, where the η^3-coordinate is normal to the body surface. The coordinates when the generic point $\boldsymbol{y}$ is over the surface are $(\eta^1, \eta^2, 0)$, and when it is at any place in the three-dimensional Euclidean space are $\boldsymbol{x} = \boldsymbol{y} + \boldsymbol{n}\delta$ where $\boldsymbol{n} = \boldsymbol{n}(\eta^1, \eta^2)$ is the exterior unit normal on the surface at the surface point $\boldsymbol{y} = \boldsymbol{y}(\eta^1, \eta^2)$, with $\boldsymbol{y} \in \mathit{\Gamma}$, while $\delta = \delta(\eta^1, \eta^2)$ is a dimensionless boundary layer thickness (or expansion parameter), with $0 < \delta \ll 1$. The Jacobian of the transformation from the (x^1, x^2, x^3) system to the (η^1, η^2, η^3) one is assumed as regular in all the domain and it is given by $J_{ij} = \partial x_i/\partial \eta_j$, for $1 \leq i, j \leq 3$, which are written as the matrix $J = [J_1\ J_2\ J_3] \in \mathbb{R}^{3\times 3}$, whose columns are

$$
\begin{aligned}
J_1 &= \frac{\partial \boldsymbol{x}}{\partial \eta^1} = \frac{\partial \boldsymbol{y}}{\partial \eta^1} + \eta^3 \frac{\partial \delta}{\partial \eta^1}\boldsymbol{n} + \eta^3 \delta \frac{\partial \boldsymbol{n}}{\partial \eta^1}\ ; \\
J_2 &= \frac{\partial \boldsymbol{x}}{\partial \eta^2} = \frac{\partial \boldsymbol{y}}{\partial \eta^2} + \eta^3 \frac{\partial \delta}{\partial \eta^2}\boldsymbol{n} + \eta^3 \delta \frac{\partial \boldsymbol{n}}{\partial \eta^2}\ ; \\
J_3 &= \frac{\partial \boldsymbol{x}}{\partial \eta^3} = \boldsymbol{n}\ \delta\ .
\end{aligned}
\tag{1}
$$

3 SPATIAL AND SURFACE METRIC TENSORS

The metric tensor is an intrinsic quantity that relates measurements performed inside a same domain, spatial or surface one. Note that here there is a spatial metric tensor g_{ij} for the three-dimensional domain, with $1 \leq i, j \leq 3$, as well as a surface metric tensor $a_{\alpha\beta}$ for the body surface, with $1 \leq \alpha, \beta \leq 2$, being the main attention in this work focused on the former one. Both of them are assumed as smooth, symmetric and positive definite tensors.

3.1 Partition of the spatial metric tensor

The spatial metric tensor can be expressed in covariant g_{ij} or in contravariant g^{ij} components, taking in the first case the form

$$
g_{ij} = \sum_{h=1}^{3} \frac{\partial x^h}{\partial \eta^i}\frac{\partial x^h}{\partial \eta^j} = \boldsymbol{x}_{,i}^T \cdot \boldsymbol{x}_{,j}\ ;
\tag{2}
$$

Covariant g_{ij}	Contravariant g^{ij}
$g_{\alpha\beta} = a_{\alpha\beta} + O(\delta)$	$g^{\alpha\beta} = a^{-1}_{\alpha\beta} + O(\delta)$
$g_{\alpha 3} = O(\delta^2)$	$g^{\alpha 3} = O(1)$
$g_{33} = \delta^2$	$g^{33} = \delta^{-2} + O(\delta^{-1})$

Table 1: Covariant g_{ij} and contravariant g^{ij} spatial metric tensor components as a function of the expansion parameter δ, with $0 < \delta \ll 1$.

where $\boldsymbol{x}_{,i} = \partial \boldsymbol{x}/\partial \eta^i$, and it can be split in surface $g_{\alpha\beta}$, normal g_{33}, and mixed $g_{\alpha 3}$, $g_{3\alpha}$ tensor components. The corresponding covariant and contravariant matrices are $\boldsymbol{g}_{ij} \equiv [g_{ij}]$ and, $\boldsymbol{g}^{ij} \equiv [g^{ij}]$, respectively, and they are related by $\boldsymbol{g}^{ij} = (\boldsymbol{g}_{ij})^{-1}$, where $(...)^{-1}$ denotes the inverse. The metric tensor partition suggests the corresponding matrix one

$$\boldsymbol{g}_{ij} = \begin{bmatrix} \boldsymbol{g}_{\alpha\beta} & \boldsymbol{g}_{\alpha 3} \\ \boldsymbol{g}_{3\beta} & g_{33} \end{bmatrix} ; \tag{3}$$

where $1 \leq i, j \leq 3$ (for the extended coordinates) and $1 \leq \alpha, \beta \leq 2$ (for the surface coordinates), with $\boldsymbol{g}_{\alpha\beta} \in \mathbb{R}^{2\times 2}$, $\boldsymbol{g}_{\alpha 3} \in \mathbb{R}^{2\times 1}$, $\boldsymbol{g}_{3\beta} \in \mathbb{R}^{1\times 2}$ and $g_{33} \in \mathbb{R}$.

3.2 Asymptotic orders in the covariant and contravariant spatial metric tensor

The asymptotic orders in the covariant g_{ij} and contravariant g^{ij} spatial metric tensor with respect to the expansion parameter δ, with $0 < \delta \ll 1$, are inferred in Appendices 8.1 1and 8.2, and they are summarized in table 1, where $a_{\alpha\beta}$ is assumed as a regular tensor.

3.3 Asymptotic orders in the Christoffel symbols

It is necessary to consider the Christoffel symbols since they appear in the expressions for the covariant derivatives. They have not a tensor character, that is, they do not transform with a tensor law under a linear coordinate transformation (see for example Smith, 1963), and they can be calculated with

$$[ij, k] \equiv \begin{bmatrix} i\, j \\ k \end{bmatrix} = \frac{1}{2}\left[\frac{\partial g_{ik}}{\partial \eta^j} + \frac{\partial g_{jk}}{\partial \eta^i} - \frac{\partial g_{ij}}{\partial \eta^k}\right] ; \tag{4}$$

for the first kind and

$$\Gamma^k_{ij} \equiv \{i, jk\} \equiv \left\{ \begin{matrix} i \\ j\ k \end{matrix} \right\} = g^{ih}[jk, h] ; \tag{5}$$

for the second kind. It is noted that, as the metric tensor g_{ij} is assumed as a symmetric tensor, these symbols are also symmetric in the lower affixes and consequently the torsion tensor $T^k_{ij} = \Gamma^k_{ij} - \Gamma^k_{ji}$ is null, that is, the spatial and surface domains are torsion-free (see for example Morgan, 1993). There are six types of these symbols depending on whether the affixes i, j, k are on the smooth surface (η^1 or η^2) or on the normal η^3 coordinate. Their asymptotic order with respect to the expansion parameter δ, with $0 < \delta \ll 1$, are estimated from the order of the spatial metric tensor in Appendices 8.5 and 8.6, and they are summarized in table 2. Note that there is only one special case given by the symbol $\{3, \beta\, \gamma\} = O(\delta^{-1})$, while the remaining ones are $O(\delta)$ or $O(\delta^2)$.

first kind	second kind
$[\alpha\beta,\gamma] = O(1)$	$\{\alpha,\beta\gamma\} = O(1)$
$[\alpha\beta,3] = O(\delta)$	$\{3,\beta\gamma\} = O(\delta^{-1})$
$[3\beta,\gamma] = O(\delta)$	$\{\beta,\alpha 3\} = O(\delta)$
$[3\beta,\gamma] = O(\delta^2)$	$\{3,\alpha 3\} = O(\delta)$
$[33,\gamma] = O(\delta^2)$	$\{\alpha,33\} = O(\delta^2)$
$[33,3] = 0$	$\{3,33\} = O(\delta^2)$

Table 2: Order of the Christoffel symbols of first and second kind as a function of the expansion parameter δ, with $0 < \delta \ll 1$.

4 NAVIER–STOKES EQUATIONS IN CURVILINEAR COORDINATES

The dimensionless Navier–Stokes equations for a laminar, isothermal and steady flow without body forces of an incompressible and viscous fluid of Newtonian type with constant physical properties, are written in the extended coordinate system (η^1,η^2,η^3) as

$$\left.\begin{aligned} u^i u^k_{,i} + g^{kj} p_{,j} &= \mathit{Re}^{-1} g^{ij} u^k_{,ij} \\ u^k_{,k} &= 0 \end{aligned}\right\} \quad ; \tag{6}$$

see for example (Aris, 1989, § 8.22); (Spurk, 1997, § 4.1.3), which are the momentum and the continuity equations, respectively, u^k is the k-component of the flow velocity expressed in contravariant components (upper index), while $\mathit{Re} = UL/\nu$ is the Reynolds number, where ν is the fluid kinematic viscosity. It should be noted that as the pressure p is a scalar field, then, its gradient can be written as $p_{,j} = \partial p/\partial\eta^j$. For further use, the first and second covariant derivatives of a smooth vector field v^k are respectively computed with (see for example (Smith, 1963, pp. 51–53))

$$\begin{aligned} v^k_{,i} &\equiv \frac{\partial v^k}{\partial \eta^i} + \left\{ \begin{matrix} k \\ h\ i \end{matrix} \right\} v^k \quad ; \\ v^k_{,ij} &\equiv \frac{\partial v^k_{,i}}{\partial \eta^j} + \left\{ \begin{matrix} k \\ h\ j \end{matrix} \right\} v^h_{,i} - \left\{ \begin{matrix} h \\ i\ j \end{matrix} \right\} v^k_{,h} \quad . \end{aligned} \tag{7}$$

4.1 Tangential component of the momentum equations

The component of the momentum equations tangential to the wall is extracted from (6) as

$$u^i u^\alpha_{,i} + g^{\alpha j} p_{,j} = \mathit{Re}^{-1} g^{ij} u^\alpha_{,ij} \quad . \tag{8}$$

In Appendix 8.3 is shown that the convective, reduced pressure and viscous terms in (8) have the asymptotic orders

$$\begin{aligned} u^i u^\alpha_{,i} &= u^3 \frac{\partial u^\alpha}{\partial \eta^3} + u^\beta u^\alpha_{,\beta} + O(\delta) \quad ; \\ g^{\alpha j} p_{,j} &= g^{\alpha\beta} p_{,\beta} + O(\delta) \quad ; \\ \mathit{Re}^{-1} g^{ij} u^\alpha_{,ij} &= \frac{\mathit{Re}^{-1}}{\delta^2} \frac{\partial^2 u^\alpha}{\partial \eta^3 \partial \eta^3} + O(\delta) \quad . \end{aligned} \tag{9}$$

Retaining the leading terms in (9), the tangential component of the momentum equations is reduced to

$$u^3 \frac{\partial u^\alpha}{\partial \eta^3} + u^\beta u^\alpha_{,\beta} + g^{\alpha\beta} p_{,\beta} = \frac{\mathit{Re}^{-1}}{\delta^2} \frac{\partial^2 u^\alpha}{\partial \eta^3 \partial \eta^3} \, . \tag{10}$$

4.2 Normal component of the momentum equations

The component of the momentum equations normal to the wall, along coordinate η^3, is taken from (6) as

$$u^i u^3_{,i} + g^{3j} p_{,j} = Re^{-1} g^{ij} u^3_{,ij} \quad . \tag{11}$$

In Appendix 8.4 it is shown that the convective, reduced pressure and viscous terms in (11) give the asymptotic orders as follows

$$\begin{aligned} u^i u^3_{,i} &= O(\delta^{-1}) \; ; \\ g^{3j} p_{,j} &= O(\delta^{-1}) \; ; \\ Re^{-1} g^{33} u^3_{,33} &= O(\delta^{-1}) \; ; \end{aligned} \tag{12}$$

and

$$\begin{aligned} u^i u^3_{,i} &= \left\{ \begin{matrix} 3 \\ \alpha\beta \end{matrix} \right\} u^\alpha u^\beta + O(1) \; ; \\ g^{3j} p_{,j} &= \frac{1}{\delta^2} \frac{\partial p}{\partial \eta^3} + O(1) \; ; \end{aligned} \tag{13}$$

respectively. Comparing (12) and (13) it follows that

$$\frac{\partial p}{\partial \eta^3} = O(\delta) \; ; \tag{14}$$

which is equivalent to the well known assumption in boundary layer analysis at zero order that the pressure gradient is negligible along the direction normal to the wall.

4.3 Continuity equation

The divergence of the velocity u^k can be computed (e.g. see Aris (1989), § 7.56) with

$$u^k_{,k} = \frac{1}{\sqrt{g^0}} \frac{\partial}{\partial x^k} \left(\sqrt{g^0} u^k \right) \; ; \tag{15}$$

since $g^0 = a^0 \delta^{-2} + O(1)$, where $g^0 = \det(g^{ij})$ and $a^0 = \det(a^{\alpha\beta})$ are the determinant of the spatial and surface metric tensors, respectively, this equation can be split and rewritten as

$$\frac{\partial u^3}{\partial \eta^3} + \frac{1}{\delta} \left(\delta \, u^\alpha \right)_{,\alpha} = 0 \quad . \tag{16}$$

4.4 Tensorial equations for a three dimensional laminar boundary layer flow

Finally, dimensionless covariant equations for a steady, laminar, attached and three dimensional boundary layer flow with null pressure gradient in the direction normal to the body surface are given collecting (10), (14) and (16),

$$\left. \begin{aligned} u^3 \frac{\partial u^\alpha}{\partial \eta^3} + u^\beta u^\alpha_{,\beta} + g^{\alpha\beta} p_{,\beta} &= \frac{Re^{-1}}{\delta^2} \frac{\partial^2 u^\alpha}{\partial \eta^3 \partial \eta^3} \\ \frac{\partial p}{\partial \eta^3} &= 0 \\ \frac{\partial u^3}{\partial \eta^3} + \frac{1}{\delta} \left(\delta \, u^\alpha \right)_{,\alpha} &= 0 \end{aligned} \right\} \quad . \tag{17}$$

In practical computations, it could be more convenient to put the pressure gradient $p_{,\alpha} = \partial p / \partial \alpha$ in the form $g^{\beta\alpha} p_{,\alpha} = v^\alpha v^\beta_{,\alpha}$, where v are the contravariant components of the outer (inviscid) velocity field, e.g. see Storti (1998).

5 PSEUDO-SPECTRAL DISCRETIZATION

The covariant three dimensional boundary layer equations given by (17) can be numerically solved using a pseudo-spectral like approach. Thorough details about this computation and other flow tests including cones, yawed flat plates and circular cylinders are given in Storti (1998), so that an account is given here mainly for the two-dimensional case. The numerical method is based on a Fourier expansion in the lateral transformed coordinate, similar to the transformation that leads to the polynomial Tchebischev expansion in finite intervals, but more appropriate to semi-infinite intervals in such a way that no extra parameter is needed for the outer boundary of the layer. A scaling is applied to the coordinate normal to the body surface with an innovation based on the computed boundary layer thickness without a variation a priori assumed for it.

5.1 Transformed equations in the two-dimensional case

When using finite differences (or finite elements) to solve Eq. (17) in a two-dimensional case (x^1, x^2), the computational domain is restricted to some region $x^2 < x^2_{\max}(x^1)$. It is evident that in order to have a uniform approximation to the two-dimensional velocity field (u^1, u^2) at all stages, $x^2_{\max}(x^1)$ should be chosen as a fixed multiple of a measure of the local nondimensional thickness, for instance, $x^2_{\max}(x^1) = M_\delta \delta^*(x^1)$, with a large M_δ (say $M_\delta \sim 5$), and δ^* the local nondimensional displacement thickness. As δ^* is not known a priori, one must guess a certain behavior for δ^*, say $\delta^*(x^1) \sim \delta_{\rm s}(x^1)$, where $\delta_{\rm s}$ is the normal scaling length, and then use $x^2_{\max}(x^1) = M_\delta \delta_{\rm s}(x^1)$. First, discrete equations are obtained as if $\delta_{\rm s}$ is a completely independent quantity chosen *a priori* and, next, $\delta_{\rm s}$ will be automatically set at the same time that the two-dimensional boundary layer equations are being solved in the time-like direction.

For numerical methods, like finite differences, it is natural to map the two-dimensional computational domain into a rectangle with an auxiliary curvilinear transformation $(x^1, x^2) \rightarrow (\eta^1, \eta^2)$. In the present case, the following transformation is selected

$$\begin{aligned} \eta^1 &= x^1 \ ; \\ \eta^2 &= \frac{x^2}{\delta_{\rm s}} \quad \text{with} \quad \delta_{\rm s} = \delta_{\rm s}(x) \ ; \end{aligned} \tag{18}$$

so that the computational domain is now the semi-infinite strip $\eta^1 > 0$ and $0 < \eta^2 < M_\delta$. This transformation is somewhat related to the similarity transformation that leads to similar solutions for wedge flows. The transformed equations in the new coordinate system are

$$\begin{aligned} v^1 \frac{\partial v^1}{\partial \eta^1} + v^2 \frac{\partial v^1}{\partial \eta^2} &= \frac{\mathit{Re}^{-1}}{{\delta_{\rm s}}^2} \frac{\partial^2 v^1}{\partial \eta^2 \partial \eta^2} + v^1_e \frac{\partial v^1_e}{\partial \eta^1} \ ; \\ \frac{1}{\delta_{\rm s}} \frac{\partial}{\partial \eta^1} (\delta_{\rm s} v^1) + \frac{\partial v^2}{\partial \eta^2} &= 0 \ ; \end{aligned} \tag{19}$$

where (v^1, v^2) are the contravariant components of the velocity vector, given by

$$\begin{aligned} v^1 &= u^1 \ ; \\ v^2 &= \frac{\partial \eta^2}{\partial x^1} u^1 + \frac{\partial \eta^2}{\partial x^2} u^2 = -\frac{x^2}{{\delta_{\rm s}}^2} \frac{\partial \delta_{\rm s}}{\partial x^1} u^1 + \frac{1}{\delta_{\rm s}} u^2 \ . \end{aligned} \tag{20}$$

It should be noticed that these equations are valid for an arbitrary choice of $\delta_{\rm s}(x^1)$. Due to the parabolic character of these boundary layer equations, the longitudinal coordinate η^1 is

solved as a *"time-like"* coordinate, whereas the normal coordinate η^2 remains as the *"spatial coordinate"*. Due to the identity $\eta^1 \equiv x^1$ in transformation (18), x^1 or η^1 is used indistinctly in the sequel. As the computational domain is the semi-infinite interval $0 \leq \eta^2 < \infty$ and the solution has a high degree of regularity, a pseudo-spectral approximation is used for η^2, whereas a standard finite difference method is applied in the time-like coordinate.

5.2 Finite interval mapping

Spectral methods are based on the approximation of the solution by a set of non-local functions, usually coming from the "spectra" of a differential operator, such that the approximation error converges faster than any finite power of the number of terms involved. The simplest example is the Fourier series for infinitely differentiable periodic functions which can be written as

$$\phi(\theta) \approx \hat{\phi}(\theta) = \sum_{k=-M}^{M} c_k \, e^{ik\theta} \, . \tag{21}$$

It is known that, if ϕ is regular enough for all θ and periodic, i.e. $\phi(\theta + 2\pi) = \phi(\theta)$, then series (21) converges faster than any power of M, i.e. $\|\phi - \hat{\phi}\| < CM^{-p}$ for any $M > M^*(p)$ and $p > 0$, which is termed as *"spectral convergence"*. For finite intervals one can extend the solution periodically to the real axis and apply this method again. Consider now the mapping

$$x^1 = (1 - \cos\theta)/2 \, . \tag{22}$$

It is simple to see that $\phi(\theta)$ preserves the same degree of continuity in the interior points as the original function. So that if ϕ has infinite continuous derivatives with respect to x^1, the same is valid with respect to θ, and a Fourier series is spectrally convergent. This is the basis of spectral approximations for finite intervals. As ϕ is even, coefficients c_k satisfy $c_k = c_{-k}$ and series (21) can be put as

$$\hat{\phi}(\theta) = \sum_{k=0}^{M} \epsilon_k c_k \, \cos k\theta = \sum_{k=0}^{M} a_k \, \cos k\theta \, ; \tag{23}$$

with $\epsilon_k = 1$ for $k = 1$ and 2 otherwise. Replacing θ in terms of x from (22) the classical expansion in Tchebyschev polynomials is obtained.

5.3 Semi-infinite intervals

For semi-infinite intervals, the domain of interest for the spectral approximation is the semi-infinite axis $0 < \eta^2 < \infty$. A first attempt is to restrain the computational domain to $0 < \eta^2 < M_\delta$, as is usual in finite differences, then apply mapping (22) combined with a linear mapping from $0 \leq x^1 \leq 1$ to $0 \leq \eta^2 \leq M_\delta$ and, finally, a Tchebyschev polynomial expansion is assumed. However, this is not efficient in the sense that the resolution is higher near the outer edge and better mappings should be considered, for instance,

$$\tanh\left(\frac{\eta^2}{\eta_s}\right) = (1 - \cos\theta)/2 \, . \tag{24}$$

The choice of an appropriate mapping involves also some degree of experience, e.g. see Storti (1998). In the numerical example, the mapping (24) with $\eta_s = 6$ was selected.

5.4 Weighted residual formulation

For the contravariant velocity component $v^1 = v^1(\eta^1)$, the multiplicative decomposition $v^1 = v^1_{\mathrm{e}}\overline{v}^1$, which satisfies $\overline{v}^1(0) = 0$ and $\overline{v}^1(\infty) = 1$, is introduced. Next, expanding $\overline{v}^1$ in the form

$$\overline{v}^1 \approx \sum_{k=0}^{M} a_k \, \cos k\theta \; ; \tag{25}$$

where the restrictions mentioned above result in two linear restrictions on the a_k coefficients

$$\begin{aligned} \overline{v}^1(0) &= \sum_{k=0}^{M} a_k = 0 \; ; \\ \overline{v}^1(\infty) &= \sum_{k=0}^{M} (-1)^k \, a_k = 0 \; ; \end{aligned} \tag{26}$$

then only $N_{\mathrm{dof}} = M - 1$ of the $M + 1$ coefficients are independent. Expansion of (25) can be put as

$$\overline{v}^1(x^1, \eta^2) = \boldsymbol{\phi}^T(\eta^2) \cdot \mathbf{a}(x^1) \; ; \tag{27}$$

where

$$\begin{aligned} \boldsymbol{\phi}^T &= \begin{bmatrix} \phi_0(\eta^2) & \phi_1(\eta^2) & \dots & \phi_k(\eta^2) \dots & \phi_M(\eta^2) \end{bmatrix} \; ; \\ \mathbf{a}^T &= \begin{bmatrix} a_0 & a_1 & \dots & a_k & \dots & a_M \end{bmatrix} \; ; \end{aligned} \tag{28}$$

with $\phi_k(\eta^2) = \cos k\theta$ and $\mathbf{a}$ is a vector of length $M + 1$ with the coefficients in the series expansion. Replacing in the continuity equation (19),

$$\begin{aligned} \frac{\partial v^2}{\partial \eta^2} &= -\frac{1}{\delta_{\mathrm{s}}} \frac{\partial}{\partial \eta^1} \left(\delta_{\mathrm{s}} v^1_{\mathrm{e}} \right) \overline{v}^1 - v^1_{\mathrm{e}} \frac{\partial \overline{v}^1}{\partial \eta^1} \\ &= -\frac{1}{\delta_{\mathrm{s}}} \frac{\partial}{\partial \eta^1} \left(\delta_{\mathrm{s}} v^1_{\mathrm{e}} \right) \overline{v}^1 - v^1_{\mathrm{e}} \boldsymbol{\phi}^T \dot{\mathbf{a}} \; ; \end{aligned} \tag{29}$$

where the dot stands for partial derivative with respect to η^1 (the time-like coordinate). Integrating in the normal direction,

$$v^2 = -\frac{1}{\delta_{\mathrm{s}}} \frac{\partial}{\partial \eta^1} \left(\delta_{\mathrm{s}} v^1_{\mathrm{e}} \right) \overline{v}^1_0 - v^1_{\mathrm{e}} \boldsymbol{\psi}^T \dot{\mathbf{a}} \; ; \tag{30}$$

where

$$\begin{aligned} \overline{v}^1_0 &= \int_0^{\eta^2} \overline{v}^1(h) \, \mathrm{d}h \; ; \\ \boldsymbol{\psi}^T &= \begin{bmatrix} \psi_0(\eta^2) & \psi_1(\eta^2) & \dots & \psi_k(\eta^2) & \dots & \psi_M(\eta^2) \end{bmatrix} \; ; \\ \psi_k &= \int_0^{\eta^2} \phi_k(h) \, \mathrm{d}h \; . \end{aligned} \tag{31}$$

Replacing (30) in the momentum equation in (19),

$$v^1 \dot{v}_{\rm e}^1[(\overline{v}^1)^2 - 1] + (v_{\rm e}^1)^2 \overline{v}^1 \boldsymbol{\phi}^T \dot{\mathbf{a}} - \\ - \left[\frac{1}{\delta_{\rm s}} \frac{\partial}{\partial \eta^1} \left(\delta_{\rm s} v_{\rm e}^1\right) \overline{v}_0^1 + v_{\rm e}^1 \boldsymbol{\psi}^T \dot{\mathbf{a}}\right] \frac{\partial v^1}{\partial \eta^2} - \frac{Re^{-1}}{{\delta_{\rm s}}^2} u_{\rm e}^1 \frac{\partial^2 \overline{v}^1}{\partial \eta^2 \eta^2} = 0 \,. \tag{32}$$

In order to obtain a system of Ordinary Differential Equations (ODE), Eq. (32) is weighted with weight functions $\{w_j\}_{j=1}^{N_{\rm dof}}$ and a system of the form

$$\mathbf{F}(\mathbf{a}, \delta_{\rm s}, \dot{\mathbf{a}}, \dot{\delta}_{\rm s}, \eta^1) = \mathbf{0} \,. \tag{33}$$

is obtained. Assume that $\delta_{\rm s}(\eta^1)$ is known a priori, for instance, $\delta_{\rm s} = c\sqrt{\eta^1}$. Then, equation (33) together with restrictions (26), is a system of $(M+1)$ Differential Algebraic Equations (DAE) with $(M+1)$ unknowns. There are $(M-1)$ ordinary differential equations plus two linear restrictions. These can be integrated by straightforwardly eliminating two of the a parameters (say a_0 and a_1) and obtaining a system of $N_{\rm dof} = M - 1$ ordinary differential equations for the "state vector" $\mathbf{a} = \begin{bmatrix} a_2 & a_3 & \dots & a_M \end{bmatrix}^T$. A standard method like Runge-Kutta or any other high order method can be used to solve it numerically. The system (33) is linear in $\dot{\mathbf{a}}$ and $\dot{\delta}_{\rm s}$ and can be put in the form

$$\mathbf{A}\dot{\mathbf{a}} + \mathbf{c}\, \dot{\delta}_{\rm s} = \mathbf{b} \,; \tag{34}$$

where all $\mathbf{A}$, $\mathbf{c}$ and $\mathbf{b}$ are functions of $\mathbf{a}$, $\delta_{\rm s}$ and x^1. Their expressions are

$$\begin{aligned} A_{jk} &= (v_{\rm e}^1)^2 \left[\int_0^\infty w_j \overline{v}^1 \phi_k \, {\rm d}\eta^2 - \int_0^\infty w_j \overline{v}^1 \frac{\partial \overline{v}^1}{\partial \eta^2} \psi_k \, {\rm d}\eta^2\right] \,; \\ c_j &= -\frac{(v_{\rm e}^1)^2}{\delta_{\rm s}} \int_0^\infty w_j \frac{\partial \overline{v}^1}{\partial \eta^2} \overline{v}_0^1 \, {\rm d}\eta^2 \,; \\ b_j &= \int_0^\infty w_j \left[-v_{\rm e}^1 \dot{v}_{\rm e}^1[(\overline{v}^1)^2 - 1] + (\dot{v}_{\rm e}^1)^2 \overline{v}_0^1 \frac{\partial \overline{v}^1}{\partial \eta^2} - \frac{Re^{-1}}{{\delta_{\rm s}}^2} v_{\rm e}^1 \frac{\partial^2 \overline{v}^1}{\partial \eta^2 \eta^2}\right] {\rm d}\eta^2 \,. \end{aligned} \tag{35}$$

5.5 Automatic normal scaling

As it was mentioned before, the normal length scale $\delta_{\rm s}$ is obtained at the same time that the system is integrated. Suppose for instance that $\delta_{\rm s}(\eta^1) = \delta^*(\eta^1)$ is set as the displacement thickness. That would mean that

$$v_{\rm e}^1 \delta^* = v_{\rm e}^1 \delta_{\rm s} \int_0^\infty (1 - \overline{v}^1) \, {\rm d}\eta^2 \,; \tag{36}$$

so that, canceling out $v_{\rm e}^1 \delta^* = v_{\rm e}^1 \delta_{\rm s}$, an additional restriction on the coefficients $\{a_k\}$ is introduced

$$\begin{aligned} 1 &= \int_0^\infty (1 - \overline{v}^1) \, {\rm d}\eta^2 = \sum_{k=0}^{M} \beta_k a_k \,; \\ \beta_k &= \int_0^\infty \left[\phi_k(\infty) - \phi_k(\eta^2)\right] \, {\rm d}\eta^2 \,. \end{aligned} \tag{37}$$

Auto-scaling consists of solving (33) with $\delta_{\rm s}$ as an additional unknown together with the restrictions (37).

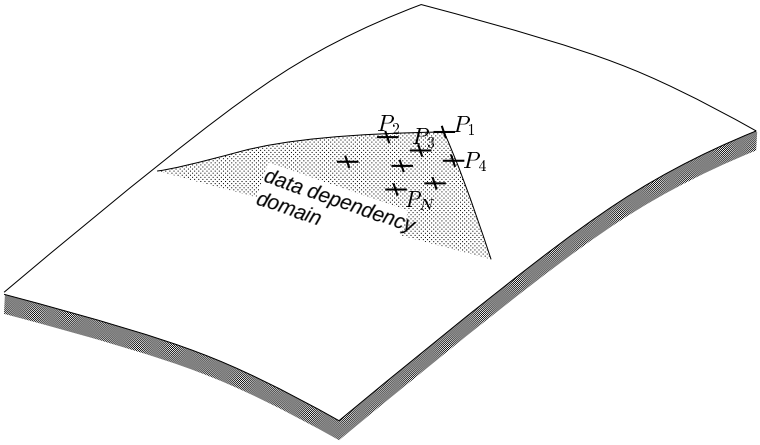

Figure 2: Mesh-less discretization on the surface.

5.6 Extension to three-dimensional surfaces

In three-dimensional surfaces there is not a direct analogy to problems of temporal evolution. In this respect, the governing equations resemble the ones for pure advection, i.e. without longitudinal and transverse diffusion, where the advected quantities are the shape parameters in the normal direction. If $\boldsymbol{\eta} = (\eta^1, \eta^2)$ is a system of intrinsic coordinates on the surface, then the pseudo-spectral discretization in the normal direction leads to a system of the form

$$\mathbf{F}\left(\frac{\partial \mathbf{w}}{\partial \eta^1}, \frac{\partial \mathbf{w}}{\partial \eta^2}, \mathbf{w}, \boldsymbol{\eta}\right) = \mathbf{0}\ ; \tag{38}$$

where $\mathbf{w}$ is the vector of shape parameters, i.e. the coefficients in the Fourier expansion of both components of the velocity vector (u^1, u^2). The *domain data dependency* is given locally by the cone including all the directions of the hodograph of the velocity at the point at the different normal positions. As this dependency cone has an aperture lower than 180^o, there is some degree of freedom in the way the solution is advanced spatially. In general, boundary layer codes use a predetermined computational grid or intrinsic coordinate system. Most of them are based on the either free streamlines, constant x planes (where x is a global Cartesian coordinate parallel to the axis of the body, this is mainly used for fuselages), or constant percentage of chord for wings. It is clear that these codes will break well before the separation point, unless the grid point arrives (by mere coincidence) parallel to the separation line at the singular separation point. Then, the system (17) is solved for a point P_1 given the data on a set of points $P_2, \ldots, P_n$ on its data dependency domain (see Fig. 2). This is equivalent to dynamically adapting the advancing front as the calculations proceed. A suitable numerical technique is the so called *mesh-less method*. Its basis is to obtain a polynomial least-squares approximation to the discrete data on points $P_1, \ldots, P_N$ and approximate the derivatives appearing in the governing equation by the derivatives of the fitting polynomial. In the case of a scalar field $\phi(x)$, let

$$\phi(\boldsymbol{\eta}) \approx \hat{\phi}(\boldsymbol{\eta}) = \sum_{k=1}^{M} a_k P_k(\boldsymbol{\eta})\ ; \tag{39}$$

be the least squares approximation. Then forming a weighted least squares error functional

$$E(\mathbf{a}) = \sum_{j=1}^{N} w_j \left[\phi_j - \hat{\phi}(\boldsymbol{\eta}_j)\right]^2\ ; \tag{40}$$

and minimizing with respect to the free parameters $\mathbf{a}$ we obtain a system of the form $\mathbf{A}\mathbf{a} = \mathbf{b}$, with

$$\begin{aligned} A_{kl} &= \sum_j w_j P_k(\boldsymbol{\eta}_j) P_l(\boldsymbol{\eta}_j) \; ; \\ b_k &= \sum_j w_j P_k(\boldsymbol{\eta}_j) \phi_j \; . \end{aligned} \tag{41}$$

Then, an approximation to $\partial\phi/\partial\eta^1$ is

$$\left.\frac{\partial \phi}{\partial \eta^1}\right|_{\boldsymbol{\eta}_i} \approx \left.\frac{\partial \hat{\phi}}{\partial \eta^1}\right|_{\boldsymbol{\eta}_i} = \sum_k a_k \left.\frac{\partial P_k}{\partial \eta^1}\right|_{\boldsymbol{\eta}_i} = \left[\frac{\partial \mathbf{P}}{\partial \eta^1}\mathbf{A}^{-1}\mathbf{W}\mathbf{P}\right]\boldsymbol{\phi} = \mathbf{c}^T\boldsymbol{\phi} \; ; \tag{42}$$

where $\mathbf{c}$ is a *"numerical stencil"* for the approximation to $\partial\phi/\partial\eta^1$. The system (38) is advanced in the following fashion. First, the numerical stencil for the approximation to $\partial\phi/\partial\eta^1$ and $\partial\phi/\partial\eta^2$ is obtained in the form

$$\begin{aligned} \frac{\partial \phi}{\partial \eta^1} &\approx \sum_{j=1}^{N} c_j^1 \phi_j \; ; \\ \frac{\partial \phi}{\partial \eta^2} &\approx \sum_{j=1}^{N} c_j^2 \phi_j \; . \end{aligned} \tag{43}$$

Then, replacing in (38) a non linear system of equations in $\mathbf{w}_j$ is obtained

$$\mathbf{F}\left(\sum_{j=1}^{N} c_j^1 \phi_j, \sum_{j=1}^{N} c_j^2 \phi_j, \mathbf{w}_j, \boldsymbol{\eta}_j\right) = \mathbf{0} \; ; \tag{44}$$

which is solved iteratively with the Newton-Raphson method. Further details are given in Storti (1998).

6 NUMERICAL EXAMPLE

As a single application of the covariant three dimensional boundary layer equations given by (17), an axially symmetric flow past a sphere of radius A is numerically solved using a pseudo-spectral like approach and the extended coordinate system on its surface. The sphere is immersed in a viscous and incompressible viscous fluid of Newtonian type, with kinematic fluid viscosity ν and fluid density ρ. The first flow case is a sphere moving with constant velocity $\boldsymbol{U}_\infty$ and no rotation, with two approximations performed for the base flow on the body surface $\boldsymbol{V} = (V^1, 0, 0)$, with $V^1 = V^1(\theta)$, where $\theta = Y^1/A$ is the polar angle from the forward stagnation point S, and Y^1 is the curvilinear coordinate along the wall measured from the same point, see figure 3 (left). The first approximation assumes the potential velocity profile $V^1 = (3/2)\, U_\infty \sin\theta$, with $0 \leq \theta \leq \pi$. The non-dimensional wall friction $\tau\sqrt{2Re_\infty}/E_\infty$ and the displacement thickness $\delta^*\sqrt{2Re_\infty}/A$ are obtained solving (17) and they are shown in figure 3 (right) as a function of the polar angle θ, where $E_\infty = \rho U_\infty^2/2$ and the exterior Reynolds number $Re_\infty = U_\infty D/\nu$ are computed using the sphere diameter $D = 2A$, with wall friction $\tau = \nu(\partial U^1/\partial Y^3)|_{Y^3=0}$, where Y^3 is the curvilinear coordinate normal to the wall, and displacement thickness δ^* computed from

$$U_\infty \delta^* = \int_0^\infty (U_\infty - U^1)\, \mathrm{d}Y^3 \; . \tag{45}$$

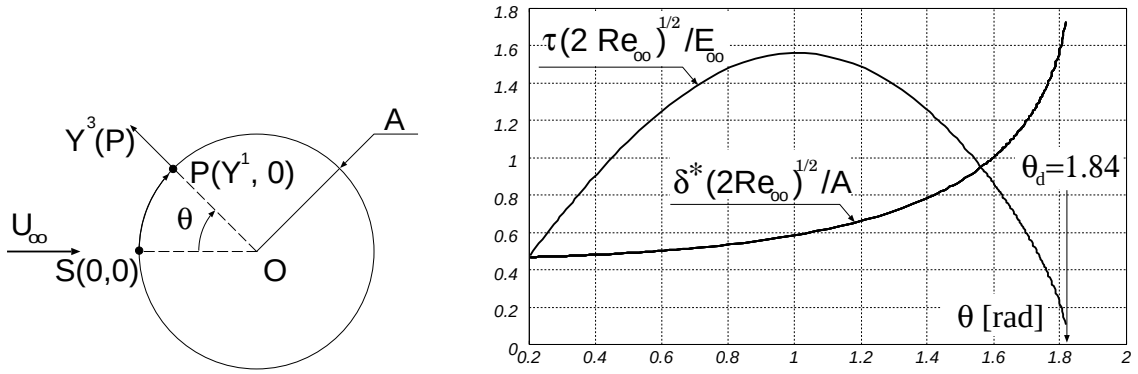

Figure 3: Right: curvilinear coordinates Y^1, Y^3 and polar angle $\theta = Y^1/A$, measured from the forward stagnation point S on a sphere of radius A, the generic point on the body surface is $P(Y^1, 0)$. Left: non-dimensional wall friction $\tau\sqrt{2Re_\infty}/E_\infty$ and displacement thickness $\delta^*\sqrt{2Re_\infty}/A$, as a function of θ using the potential velocity profile. The separation point is at $\theta_d \approx 1.84$ radians ($\approx 105.45°$).

The separation point is found at $\theta_d \approx 1.84$ radians ($\approx 105.45°$), in good agreement with the separation predictions given by a Rott-Cratree semi-analytical and a finite-difference computations, being between $103.6°$ and $105.5°$, respectively, as cited by White (2005).

On the other hand, for super-critical Reynolds numbers, the experimental velocity profile does not differ too much from the potential flow model but there are flow separation effects. Since in the axially symmetrical Blasius profile series is known up to the term θ^7, the term $\sin\theta$ is replaced by a series in odd powers giving a more realistic velocity profile. Thus, the actual velocity profile measured by Fage (1936) and also cited by White (2005) at $Re = 200\ 000$ fits the curve

$$\frac{U}{U_\infty} = \frac{3}{2}\,\theta - 0.4371\,\theta^3 + 0.1481\,\theta^5 - 0.0423\,\theta^7 \quad ; \tag{46}$$

for $0 \leq \theta \leq 1.48$, which drops off much faster than the potential one, reaching a maximum of $U/U_\infty = 1.274$ at $\theta = 1.291$ radians ($\approx 74°$) while the potential velocity profile has a maximum of $U/U_\infty = 3/2$ at $\theta = 1.571$ radians ($\approx 90°$). The flow separation is now reached at $\theta''_d = 1.424$ radians ($\approx 81.6°$), which is again in good agreement with the predictions given by a Rott-Cratree semi-analytical and a finite-difference computation, being between $81.1°$ and $82.4°$, respectively.

In the second flow case, the velocity profile given by (46) is again assumed, but now the sphere is rotating with a steady spin rotation $\boldsymbol{\omega}$ around an axis parallel to the constant velocity $\boldsymbol{U}_\infty$, such that $\omega A/U_\infty = 1$. It is verified that whereas the inviscid streamlines are simply meridians, the limit viscous streamlines in this case have a tendency to rotate with the rotating sphere, until they align with the separation streamline that is a parallel at $\theta'''_d = 1.47$ radians ($\approx 84.2°$) from the forward stagnation point, as is shown in figure 4. Note that the spinning tends to stabilize the boundary layer against separation, resulting in a delay of almost 3 degrees with respect to $\theta''_d = 1.424$ radians ($\approx 81.6°$). This is due to the centrifugal force that can be assimilated to a pressure gradient directed to the equator $\theta \to \pi/2$ radians ($\theta \to 90°$). Since the separation for the sphere happens before the equator this is equivalent to a favorable pressure gradient which has also a significant incidence in the viscous drag.

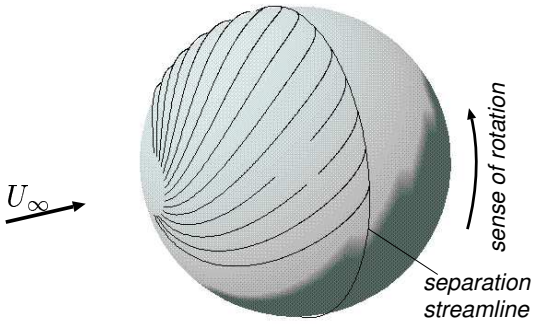

Figure 4: Computed limit viscous streamlines for the sphere of radius A, moving with a steady spin rotation ω around an axis parallel to the constant velocity $\boldsymbol{U}_\infty$, when $\omega A/U_\infty = 1$.

7 CONCLUSIONS

An attached, laminar, isothermal steady flow without body forces of an incompressible viscous fluid of Newtonian type and constant physical properties has been considered. The boundary layer equations were first written in orthogonal extended curvilinear three-dimensional coordinates η^i, with $i = 1, 2, 3$. Next, the approximation for the two-dimensional surface coordinates η^α, with $\alpha = 1, 2$, were derived from the asymptotic properties of the metric tensor g^{ij} with respect to the dimensionless boundary layer thickness $\delta(\eta^1, \eta^2)$, with $0 < \delta \ll 1$. Six types of Christoffel symbols were found, depending on whether the affixes i, j, k are over the smooth surface, η^1 and η^2, or along the normal direction η^3. The order of these symbols with respect to the expansion parameter δ were estimated from the corresponding ones of the metric tensor, which are summarized in table 2. The well known assumption that the pressure gradient in the normal direction to the surface is null, it is recovered in the continuity equation (second line in (17)). As a practical application, the boundary layer near a sphere in an axisymmetrical steady flow was modeled using the covariant form (17) and numerically computed using a pseudo-spectral approach. From a practical point of view, some advantages of writing the boundary layer equations in a covariant formalism are:

1. It is easy to check the physical consistence and to detect errors due to the approximations performed in the derivations;
2. There is no explicit curvature terms and it only remains the surface metric tensor a^{ij} in the continuity equation;
3. Any curvature term is placed only in the covariant derivatives rather than displayed in the equations in order to obtain a more physical picture and easier verification;
4. It is easier to change from one coordinate system to another since there are not complicated terms due to curvature effects;
5. These equations are covariant under a linear coordinate transformation on the two intrinsic surface coordinates η^1, η^2, and an arbitrary scaling of the coordinate η^3 normal to the body surface;
6. If they are written as conservative equations then they remain as conservatives;
7. Finally, the covariant form also shows a diffusive character on the coordinate η^3 normal to the body surface and a wave-like one on the intrinsic surface coordinates η^1, η^2, that is, it has a dual intrinsic parabolic-hyperbolic nature.

Acknowledgments

This work has received financial support from Consejo Nacional de Investigaciones Cientficas y Tcnicas (CONICET, Argentina, grants PIP 02552/00, PIP 5271/05), Universidad Nacional del Litoral (UNL, Argentina, grant CAI+D 2005-10-64) and Agencia Nacional de Promocin Cientfica y Tecnolgica (ANPCyT, Argentina, grants PICT 12-14573/2003, PME 209/2003, PICT 1506/2006) and was partially performed with the *Free Software Foundation/ GNU-Project* resources as GNU/Linux OS and GNU/Octave, as well as other Open Source resources as TGif and LaTeX.

8 APPENDIX

8.1 Asymptotic orders in the covariant spatial metric tensor

For a point $\boldsymbol{y} \in \Gamma$, the partial derivatives $\boldsymbol{y}_{,1}$, $\boldsymbol{y}_{,2}$ are parallel to the surface Γ and, in the same way, the partial derivatives $\boldsymbol{n}_{,1}$ and $\boldsymbol{n}_{,2}$ are also parallel to the surface Γ, Therefore, their scalar product with respect to the unit normal to the body surface $\boldsymbol{n}$ are nulls, i.e. $\langle \partial \boldsymbol{y}^T / \partial \eta^\alpha, \boldsymbol{n} \rangle = 0$ and $\langle \partial \boldsymbol{n}^T / \partial \eta^\alpha, \boldsymbol{n} \rangle = 0$. There are three types of components in the covariant metric tensor g_{ij}: surface, mixed and normal components. First, the surface components $g_{\alpha\beta}$ are written as

$$\begin{aligned} g_{\alpha\beta} &= \frac{\partial \boldsymbol{x}^T}{\partial \eta^\alpha} \cdot \frac{\partial \boldsymbol{x}}{\partial \eta^\beta} \\ &= \frac{\partial \boldsymbol{y}^T}{\partial \eta^\alpha} \cdot \frac{\partial \boldsymbol{y}}{\partial \eta^\beta} + 2\eta^3 \frac{\partial \boldsymbol{y}^T}{\partial \eta^\alpha} \cdot \frac{\partial \boldsymbol{n}}{\partial \eta^\beta}\, \delta + \left(\eta^3\right)^2 \frac{\partial \boldsymbol{n}^T}{\partial \eta^\alpha} \cdot \frac{\partial \boldsymbol{n}}{\partial \eta^\beta}\, \delta^2 + \left(\eta^3\right)^2 \frac{\partial \delta}{\partial \eta^\alpha} \frac{\partial \delta}{\partial \eta^\beta} \\ &= a_{\alpha\beta} + 2\eta^3 b_{\alpha\beta}\, \delta + \left(\eta^3\right)^2 c_{\alpha\beta}\, \delta^2 + \left(\eta^3\right)^2 d_{\alpha\beta} = a_{\alpha\beta} + O(\delta)\ ; \end{aligned} \tag{47}$$

where

$$\begin{bmatrix} a_{\alpha\beta} & b_{\alpha\beta} \\ c_{\alpha\beta} & d_{\alpha\beta} \end{bmatrix} = \begin{bmatrix} \langle \boldsymbol{y}_{,\alpha}^T, \boldsymbol{y}_{,\beta} \rangle & \langle \boldsymbol{y}_{,\alpha}^T, \boldsymbol{n}_{,\beta} \rangle \\ \langle \boldsymbol{n}_{,\alpha}^T, \boldsymbol{n}_{,\beta} \rangle & \delta_{,\alpha} \delta_{,\beta} \end{bmatrix} \tag{48}$$

which are functions of the surface coordinates η^1, η^2. The first term $a_{\alpha\beta}$ gives the intrinsic components of the surface metric tensor. Note from (47) that near the surface the components of the metric tensor $g_{\alpha\beta}$ are equal, at first order, to the intrinsic $a_{\alpha\beta}$ ones. Next, the mixed components $g_{\alpha 3}$ are written as

$$g_{\alpha 3} = \frac{\partial \boldsymbol{x}^T}{\partial \eta^\alpha} \cdot \frac{\partial \boldsymbol{x}}{\partial \eta^3} = \eta^3 \frac{\partial \delta}{\partial \eta^\alpha}\, \delta = O(\delta^2)\ . \tag{49}$$

Finally, the normal component g_{33}, which is reduced to

$$g_{33} = \frac{\partial \boldsymbol{x}^T}{\partial \eta^3} \cdot \frac{\partial \boldsymbol{x}}{\partial \eta^3} = \boldsymbol{n}\delta \cdot \boldsymbol{n}\delta = \delta^2\ . \tag{50}$$

Then, using the asymptotic orders given by (47,49,50), the covariant metric tensor, expressed in matrix notation and partitioned as in (3), has the asymptotic expansion

$$\boldsymbol{g}_{ij} = [g_{ij}] = \begin{bmatrix} \boldsymbol{a}_{\alpha\beta} + O(\delta) & O(\delta^2) \\ O(\delta^2) & \delta^2 \end{bmatrix} = \mathsf{S}\mathsf{T}\mathsf{S}\ ; \tag{51}$$

where $\boldsymbol{a}_{\alpha\beta} = [a_{\alpha\beta}] \in \mathbb{R}^{2\times 2}$, while $\mathsf{T}, \mathsf{S} \in \mathbb{R}^{3\times 3}$, with

$$\mathsf{T} = \begin{bmatrix} \boldsymbol{a}_{\alpha\beta} + O(\delta) & O(\delta) \\ O(\delta) & 1 \end{bmatrix} \quad \text{and} \quad \mathsf{S} = \operatorname{diag}\{1, 1, \delta\}\ ; \tag{52}$$

where S is a regular matrix whether $\delta > 0$. Then, the first column of table 1 is obtained from (51).

8.2 Asymptotic orders in the contravariant spatial metric tensor

Using matrix notation, the contravariant metric tensor g^{ij} is computed from the covariant g_{ij} one using the relation $g^{ij} = (g_{ij})^{-1}$. For this aim, it is convenient to introduce the decomposition

$$T = T_1 + T_2 \quad \text{with } T_1 = \begin{bmatrix} \boldsymbol{a}_{\alpha\beta} & 0 \\ 0 & 1 \end{bmatrix} \quad \text{and} \quad T_2 = \begin{bmatrix} O(\delta) & O(\delta) \\ O(\delta) & 0 \end{bmatrix} ; \tag{53}$$

where $T^{-1} = \mathrm{diag}\{\boldsymbol{a}^{-1}_{\alpha\beta}, 1\}$ is regular if $a_{\alpha\beta}$ also is. Then, using (51, 53),

$$\begin{aligned} g^{ij} &= [g^{ij}] = S^{-1} T^{-1} S^{-1} \\ &= S^{-1} T_1^{-1} \left(I + T_2 T_1^{-1}\right)^{-1} S^{-1} \\ &= S^{-1} T_1^{-1} \left(I - T_2 T_1^{-1} + (T_2 T_1^{-1})^2 + ...\right)^{-1} S^{-1} \\ &= S^{-1} \left[T_1^{-1} + O(\delta)\right] S^{-1} \\ &= \mathrm{diag}\{1, 1, \delta^{-1}\} \begin{bmatrix} \boldsymbol{a}^{-1}_{\alpha\beta} + O(\delta) & O(\delta) \\ O(\delta) & 1 + O(\delta) \end{bmatrix} \mathrm{diag}\{1, 1, \delta^{-1}\} \\ &= \begin{bmatrix} \boldsymbol{a}^{-1}_{\alpha\beta} + O(\delta) & O(1) \\ O(1) & \delta^{-2} + O(\delta^{-1}) \end{bmatrix} ; \end{aligned} \tag{54}$$

where the last line in (54) produces the second column of table 1.

8.3 Asymptotic orders in the tangential component of the momentum equation

The asymptotic orders in the component of the momentum equation tangential to the surface (η^1, η^2) are determined as follows. First, the convective acceleration is given by

$$u^i u^\gamma_{,i} = u^\alpha u^\gamma_{,\alpha} + u^3 \frac{\partial u^\gamma}{\partial \eta^3} + u^3 u^h \left\{ \begin{matrix} \gamma \\ h\ 3 \end{matrix} \right\} = u^\alpha u^\gamma_{,\alpha} + u^3 \frac{\partial u^\gamma}{\partial \eta^3} + O(\delta) ; \tag{55}$$

Next, the reduced pressure gradient is split in normal and tangential components, and taken into account the second line of (66),

$$g^{\alpha j} \frac{\partial p}{\partial \eta^j} = g^{\alpha\beta} \frac{\partial p}{\partial \eta^\beta} + g^{\alpha 3} \frac{\partial p}{\partial \eta^3} = g^{\alpha\beta} \frac{\partial p}{\partial \eta^\beta} + O(1) O(\delta) = g^{\alpha\beta} \frac{\partial p}{\partial \eta^\beta} + O(\delta) . \tag{56}$$

Finally, for the viscous dissipation, the first covariant derivative of u^γ is given by

$$u^\gamma_{,i} = \frac{\partial u^\gamma}{\partial \eta^i} + \left\{ \begin{matrix} \gamma \\ h\ i \end{matrix} \right\} u^h \quad . \tag{57}$$

As in the $\{\gamma, h\ i\}$ symbol the special one $\{3, \beta\ \gamma\}$ is not present, all the velocities u^h are assumed of $O(1)$, and taking into account the asymptotic values in table 1, it follows that

$$u^\gamma_{,i} = \frac{\partial u^\gamma}{\partial \eta^i} + O(\delta) ; \tag{58}$$

and from (58), when $i = 3$,

$$\frac{\partial u^\gamma_{,3}}{\partial \eta^3} = \frac{\partial^2 u^\gamma}{\partial \eta^3 \partial \eta^3} + O(\delta) . \tag{59}$$

The second covariant derivative of the tangential velocity u^γ is

$$u^\gamma_{,ij} = \frac{\partial u^\gamma_{,i}}{\partial \eta^j} \left\{ \begin{matrix} \gamma \\ h\ j \end{matrix} \right\} u^h_{,i} \left\{ \begin{matrix} h \\ i\ j \end{matrix} \right\} u^\gamma_{,h} \quad ; \tag{60}$$

in the first symbol on the r.h.s., the special case $\{3, \beta\gamma\}$ is not present either except for the second symbol. There are four cases to be considered:

1. when i, j run over $\{1, 2\}$,

$$\begin{aligned} u^\gamma_{,\alpha\beta} &= \frac{\partial u^\gamma_{,\alpha}}{\partial \eta^\beta} + \left\{ \begin{matrix} \gamma \\ h\ \beta \end{matrix} \right\} u^h_{,\alpha} - \left\{ \begin{matrix} h \\ \alpha\ \beta \end{matrix} \right\} u^\gamma_{,h} \\ &= \frac{\partial u^\gamma_{,\alpha}}{\partial \eta^\beta} + \left\{ \begin{matrix} \gamma \\ \lambda\ \beta \end{matrix} \right\} u^\lambda_{,\alpha} + \left\{ \begin{matrix} \gamma \\ 3\ \beta \end{matrix} \right\} u^3_{,\alpha} - \left\{ \begin{matrix} \lambda \\ \alpha\ \beta \end{matrix} \right\} u^\gamma_{,\lambda} - \left\{ \begin{matrix} 3 \\ \alpha\ \beta \end{matrix} \right\} u^\gamma_{,3} \\ &= O(1) + O(1) + O(\delta) + O(1) + O(\delta^{-1}) \\ &= O(\delta^{-1}) \quad \text{and} \quad g^{\alpha\beta} = O(1) \quad ; \end{aligned} \tag{61}$$

2. when $i = 3$ and $j \neq 3$,

$$\begin{aligned} u^\gamma_{,3\beta} &= \frac{\partial u^\gamma_{,3}}{\partial \eta^\beta} + \left\{ \begin{matrix} \gamma \\ h\ \beta \end{matrix} \right\} u^h_{,3} - \left\{ \begin{matrix} h \\ 3\ \beta \end{matrix} \right\} u^\gamma_{,h} \\ &= \frac{\partial u^\gamma_{,3}}{\partial \eta^\beta} + \left\{ \begin{matrix} \gamma \\ \lambda\ \beta \end{matrix} \right\} u^\lambda_{,3} + \left\{ \begin{matrix} \gamma \\ 3\ \beta \end{matrix} \right\} u^3_{,3} - \left\{ \begin{matrix} \lambda \\ 3\ \beta \end{matrix} \right\} u^\gamma_{,\lambda} - \left\{ \begin{matrix} 3 \\ 3\ \beta \end{matrix} \right\} u^\gamma_{,3} \\ &= O(1) + O(\delta) + O(\delta) + O(\delta) \\ &= O(1) \quad \text{and} \quad g^{3j} = O(1) \quad ; \end{aligned} \tag{62}$$

3. the case $i \neq 3$ and $j = 3$ is analogous to previous one;
4. finally when $i = j = 3$,

$$\begin{aligned} u^\gamma_{,33} &= \frac{\partial u^\gamma_{,3}}{\partial \eta^3} + \left\{ \begin{matrix} \gamma \\ h\ 3 \end{matrix} \right\} u^h_{,3} - \left\{ \begin{matrix} h \\ 3\ 3 \end{matrix} \right\} u^\gamma_{,h} \\ &= \frac{\partial u^\gamma_{,3}}{\partial \eta^3} + \left\{ \begin{matrix} \gamma \\ \lambda\ 3 \end{matrix} \right\} u^\lambda_{,3} + \left\{ \begin{matrix} 3 \\ 3\ 3 \end{matrix} \right\} u^3_{,3} - \left\{ \begin{matrix} \lambda \\ 3\ 3 \end{matrix} \right\} u^\gamma_{,\lambda} - \left\{ \begin{matrix} 3 \\ 3\ 3 \end{matrix} \right\} u^\gamma_{,3} \\ &= O(1) + O(\delta) + O(\delta^2)O(\delta^2) + O(\delta^2) + O(\delta^2) \\ &= O(1) \quad \text{and} \quad g^{33} = O(\delta^{-2}) \quad . \end{aligned} \tag{63}$$

Collecting (59), (61) and (63), and using the standard assumption that the non-dimensional boundary layer thickness grows as $\delta = O(1/\sqrt{Re})$ which, in turn, is equivalent to $Re^{-1} = O(\delta^2)$, the dissipation of the tangential momentum is reduced to

$$Re^{-1} g^{ij} u^\gamma_{,ij} = \frac{Re^{-1}}{\delta^2} u^\gamma_{,33} + Re^{-1} O(\delta^{-1}) = \frac{Re^{-1}}{\delta^2} \frac{\partial^2 u^\gamma}{\partial \eta^3 \partial \eta^3} + O(1) \, . \tag{64}$$

8.4 Asymptotic orders in the normal component of the momentum equation

The asymptotic orders in the component of the momentum equation normal to the wall direction η^3 are determined as follows:

1. The convective acceleration is given by

$$\begin{aligned} u^i u^3_{,i} &= u^i \frac{\partial u^3}{\partial \eta^i} + \left\{ \begin{matrix} 3 \\ h\ i \end{matrix} \right\} u^h u^i = u^i \frac{\partial u^3}{\partial \eta^i} + \left\{ \begin{matrix} 3 \\ \alpha\ \beta \end{matrix} \right\} u^\alpha u^\beta + \left\{ \begin{matrix} 3 \\ 3\ 3 \end{matrix} \right\} u^3 u^3 \ ; \\ &= O(1) + O(\delta^{-1}) + O(\delta^2) + O(\delta) = O(\delta^{-1}) \ ; \end{aligned} \tag{65}$$

2. The reduced pressure gradient is decomposed as

$$\begin{aligned} g^{3j} \frac{\partial p}{\partial \eta^j} &= g^{33} \frac{\partial p}{\partial \eta^3} + g^{3\alpha} \frac{\partial p}{\partial \eta^\alpha} = \frac{1}{\delta^2} \frac{\partial p}{\partial \eta^3} + O(1) O(1) = O(\delta^{-1}) \quad ; \\ \text{while} \qquad \frac{\partial p}{\partial \eta^3} &= O(\delta) \quad . \end{aligned} \tag{66}$$

3. For the viscous dissipation, the first covariant derivative of the normal velocity u^3 is given by

$$u^3_{,i} = \frac{\partial u^3}{\partial \eta^i} + \left\{ \begin{matrix} 3 \\ h\ i \end{matrix} \right\} u^h \ ; \tag{67}$$

which is split as

$$u^3_{,3} = \frac{\partial u^3}{\partial \eta^3} + \left\{ \begin{matrix} 3 \\ h\ 3 \end{matrix} \right\} u^h = O(1) + O(\delta) = O(1) \ ; \tag{68}$$

and

$$u^3_{,\alpha} = \frac{\partial u^3}{\partial \eta^\alpha} + \left\{ \begin{matrix} 3 \\ \gamma\ \alpha \end{matrix} \right\} u^\gamma + \left\{ \begin{matrix} 3 \\ 3\ \alpha \end{matrix} \right\} u^3 = O(1) + O(\delta^{-1}) + O(\delta) = O(\delta^{-1}) \ ; \tag{69}$$

and the first covariant derivative of the tangential velocity u^γ is given by

$$\begin{aligned} u^\gamma_{,3} &= \frac{\partial u^\gamma}{\partial \eta^3} + \left\{ \begin{matrix} \gamma \\ h\ 3 \end{matrix} \right\} u^h = \frac{\partial u^\gamma}{\partial \eta^3} + \left\{ \begin{matrix} \gamma \\ \lambda\ 3 \end{matrix} \right\} u^\lambda + \left\{ \begin{matrix} \gamma \\ 3\ 3 \end{matrix} \right\} u^3 \\ &= O(1) + O(\delta) + O(\delta^2) = O(1) \ . \end{aligned} \tag{70}$$

The second covariant derivative of the normal velocity u^3 is

$$u^3_{,ij} = \frac{\partial u^3_{,i}}{\partial \eta^j} + \left\{ \begin{matrix} 3 \\ h\ j \end{matrix} \right\} u^h_{,i} - \left\{ \begin{matrix} h \\ i\ j \end{matrix} \right\} u^3_{,h} \ . \tag{71}$$

There are four cases to be considered:

(a) when i, j run over $\{1, 2\}$,

$$\begin{aligned} u^3_{,\alpha\beta} &= \frac{\partial u^3_{,\alpha}}{\partial \eta^\beta} + \left\{ \begin{matrix} 3 \\ h\ \beta \end{matrix} \right\} u^h_{,\alpha} - \left\{ \begin{matrix} h \\ \alpha\ \beta \end{matrix} \right\} u^3_{,h} \\ &= \frac{\partial u^3_{,\alpha}}{\partial \eta^\beta} + \left\{ \begin{matrix} 3 \\ \lambda\ \beta \end{matrix} \right\} u^\lambda_{,\alpha} + \left\{ \begin{matrix} 3 \\ 3\ \beta \end{matrix} \right\} u^3_{,\alpha} - \left\{ \begin{matrix} \lambda \\ \alpha\ \beta \end{matrix} \right\} u^3_{,\lambda} - \left\{ \begin{matrix} 3 \\ \alpha\ \beta \end{matrix} \right\} u^3_{,3} \\ &= O(1) + O(\delta^{-1}) O(1) + O(\delta) O(\delta^{-1}) + O(1) O(\delta^{-1}) + O(\delta^{-1}) O(1) \\ &= O(\delta^{-1}) \quad \text{and} \quad g^{\alpha\beta} = O(1) \quad ; \end{aligned} \tag{72}$$

(b) when $i = 3$ and $j \neq 3$,

$$\begin{aligned} u^3_{,3\beta} &= \frac{\partial u^3_{,3}}{\partial \eta^\beta} + \left\{ \begin{matrix} 3 \\ h\ \beta \end{matrix} \right\} u^h_{,3} - \left\{ \begin{matrix} h \\ 3\ \beta \end{matrix} \right\} u^3_{,h} \\ &= \frac{\partial u^3_{,3}}{\partial \eta^\beta} + \left\{ \begin{matrix} 3 \\ \lambda\ \beta \end{matrix} \right\} u^\lambda_{,3} + \left\{ \begin{matrix} 3 \\ 3\ \beta \end{matrix} \right\} u^3_{,3} - \left\{ \begin{matrix} \lambda \\ 3\ \beta \end{matrix} \right\} u^3_{,\lambda} - \left\{ \begin{matrix} 3 \\ 3\ \beta \end{matrix} \right\} u^3_{,3} \\ &= O(1) + O(\delta^{-1})O(1) + O(\delta^2)O(1) + O(\delta^2)O(1) + O(\delta^2)O(1) \\ &= O(\delta^{-1}) \quad \text{and} \quad g^{3j} = O(1) \quad ; \end{aligned} \tag{73}$$

(c) the case $i \neq 3$ and $j = 3$ is analogous to previous one;
(d) finally when $i = j = 3$,

$$\begin{aligned} u^3_{,33} &= \frac{\partial u^3_{,3}}{\partial \eta^3} + \left\{ \begin{matrix} 3 \\ h\ 3 \end{matrix} \right\} u^h_{,3} - \left\{ \begin{matrix} h \\ 3\ 3 \end{matrix} \right\} u^3_{,h} \\ &= \frac{\partial u^3_{,3}}{\partial \eta^3} + \left\{ \begin{matrix} 3 \\ \lambda\ 3 \end{matrix} \right\} u^\lambda_{,3} + \left\{ \begin{matrix} 3 \\ 3\ 3 \end{matrix} \right\} u^3_{,3} - \left\{ \begin{matrix} \lambda \\ 3\ 3 \end{matrix} \right\} u^3_{,\lambda} - \left\{ \begin{matrix} 3 \\ 3\ 3 \end{matrix} \right\} u^3_{,3} \\ &= O(1) + O(\delta)O(1) + O(\delta^2)O(1) + O(\delta^2)O(1) + O(\delta^2)O(1) \\ &= O(1) \quad \text{and} \quad g^{33} = O(\delta^{-2}) \quad . \end{aligned} \tag{74}$$

Collecting (72), (73) and (74), and using again the standard assumption $Re^{-1} = O(\delta^2)$, the dissipation of the normal momentum is reduced to

$$Re^{-1} g^{ij} u^3_{,ij} = O(\delta^2)\ O(\delta^{-2})\ O(\delta^{-1}) = O(\delta^{-1}) \ . \tag{75}$$

8.5 Asymptotic orders in the Christoffel symbols of first kind

The Christoffel symbols of first kind are calculated with

$$[ij, k] = \frac{1}{2} \left[\frac{\partial g_{ik}}{\partial \eta^j} + \frac{\partial g_{jk}}{\partial \eta^i} - \frac{\partial g_{ij}}{\partial \eta^k} \right] \ ; \tag{76}$$

there are six types of these symbols depending on whether the affixes i, j, k are over the smooth surface (η^1 or η^2), or along the normal η^3. The order of these symbols with respect to the expansion parameter δ, with $0 < \delta \ll 1$, are estimated from the order of the metric tensor as given in (77).

$$\begin{aligned} 2\ [\alpha\beta, \gamma] &= \frac{\partial g_{\alpha\gamma}}{\partial \eta^\beta} + \frac{\partial g_{\beta\gamma}}{\partial \eta^\alpha} - \frac{\partial g_{\alpha\beta}}{\partial \eta^\gamma} = O(1) + O(1) + O(1) = O(1) \quad ; \\ 2\ [\alpha\beta, 3] &= \frac{\partial g_{\alpha 3}}{\partial \eta^\beta} + \frac{\partial g_{\beta 3}}{\partial \eta^\alpha} - \frac{\partial g_{\alpha\beta}}{\partial \eta^3} = O(\delta^2) + O(\delta^2) - \frac{\partial}{\partial \eta^3} \left[a_{\alpha\beta} + \eta^3 O(\delta) \right] = O(\delta) \quad ; \\ 2\ [\alpha 3, \beta] &= \frac{\partial g_{\alpha\beta}}{\partial \eta^3} + \frac{\partial g_{3\beta}}{\partial \eta^\alpha} - \frac{\partial g_{\alpha 3}}{\partial \eta^\beta} = O(\delta) + O(\delta^2) - O(\delta^2) = O(\delta) \quad ; \\ 2\ [3\beta, 3] &= \frac{\partial g_{33}}{\partial \eta^\beta} + \frac{\partial g_{\beta 3}}{\partial \eta^3} - \frac{\partial g_{3\beta}}{\partial \eta^3} = \frac{\partial g_{33}}{\partial \eta^\beta} = \frac{\partial \delta^2}{\partial \eta^\beta} = O(\delta^2) \quad ; \\ 2\ [33, \gamma] &= \frac{\partial g_{3\gamma}}{\partial \eta^3} + \frac{\partial g_{3\gamma}}{\partial \eta^3} - \frac{\partial g_{33}}{\partial \eta^\gamma} = O(\delta^2) \quad ; \\ 2\ [33, 3] &= \frac{\partial g_{33}}{\partial \eta^3} + \frac{\partial g_{33}}{\partial \eta^3} - \frac{\partial g_{33}}{\partial \eta^3} = \frac{\partial g_{33}}{\partial \eta^3} = 0 \quad . \end{aligned} \tag{77}$$

8.6 Asymptotic orders in the Christoffel symbols of second kind

The order of Christoffel symbols of second kind related to the expansion parameter δ, with $0 < \delta \ll 1$, is also determined from the order of the metric tensor, as follows

$$\begin{aligned}
\{\alpha, \beta\gamma\} &= g^{\alpha\mu}[\beta\gamma, \mu] + g^{\alpha 3}[\beta\gamma, 3] = O(1)\, O(1) + O(1)\, O(\delta) = O(1) \quad ; \\
\{3, \beta\gamma\} &= g^{3\mu}[\beta\gamma, \mu] + g^{33}[\beta\gamma, 3] = O(1)\, O(1) + O(\delta^{-2})\, O(\delta) = O(\delta^{-1}) \quad ; \\
\{\beta, \alpha 3\} &= g^{\beta\mu}[\alpha 3, \mu] + g^{\beta 3}[\alpha 3, 3] = O(1)\, O(\delta) + O(1)\, O(\delta^2) = O(\delta) \quad ; \\
\{3, \alpha 3\} &= g^{3\mu}[\alpha 3, \mu] + g^{33}[\alpha 3, 3] = O(1)\, O(\delta) + O(\delta^{-2})\, O(\delta^2) = O(\delta) \quad ; \\
\{\alpha, 33\} &= g^{\alpha\mu}[33, \mu] + g^{\alpha 3}[33, 3] = O(1)\, O(\delta^2) + g^{\alpha 3} 0 = O(\delta^2) \quad ; \\
\{3, 33\} &= g^{3\mu}[33, \mu] + g^{33}[33, 3] = O(1)\, O(\delta^2) + g^{33} 0 = O(\delta^2) \quad .
\end{aligned} \tag{78}$$

Note that in (78) there is only one special case given by the symbol $\{3, \beta\ \gamma\} = O(\delta^{-1})$, while the remaining ones are $O(\delta)$ or $O(\delta^2)$, and that $\{\alpha, j\ k\} = O(\delta)$.

REFERENCES

Anderson O.L. Calculation of three–dimensional boundary layers on rotating turbine blades. In A. Hamed, J. Herring, and L. Povinelli, editors, *Three–dimensional Flow Phenomena in Fluid Machinery*, volume 32, pages 121–132. ASME, 1985.

Aris R. *Vector, tensors, and the basic equations of fluid mechanics*. Dover, 1989.

Battaglia L., D'Elía J., Storti M.A., and Nigro N.M. Numerical simulation of transient free surface flows. *ASME-Journal of Applied Mechanics*, 73(6):1017–1025, 2006.

Bermúdez L., Velázquez A., and Matesanz A. Viscous–inviscid method for the simulation of turbulent unsteady wind turbine airfoil flow. *Journal of Wind Engineering and Industrial Aerodynamics*, 90:643–661, 2002.

Bogdanov A.N. and Diyesperov V.N. The simulation of unsteady transonic flow and the stability of a transonic boundary layer. *Journal of Applied Mathematics and Mechanics*, 69:358–365, 2005.

Cebeci T. and Cousteix J. *Modeling and computation of boundary-layer flows*. Springer-Verlag, 1999.

D'Elía J., Nigro N., and Storti M. Numerical simulations of axisymmetric inertial waves in a rotating sphere by finite elements. *International Journal of Computational Fluid Dynamics*, 20(10):673–685, 2006.

D'Elía J., Storti M.A., and Idelsohn S.R. A panel-Fourier method for free surface methods. *ASME-Journal of Fluids Engineering*, 122(2):309–317, 2000.

Dey J. Constant pressure laminar, transitional and turbulent flows. an approximate unified treatment. *ASME Journal of Fluids Engineering*, pages 806–808, 2001.

Dwoyer D.L., Lewis C.H., and Gogineni P.R. A procedure for calculating laminar, transitional and/or turbulent three-dimensional boundary layers including surface curvature effects about arbitrary blunt-nosed bodies. In *Aerospace Sciences Meeting*. AIAA, Huntsville, Ala., 1978.

Epureanu B.I., Hall K.C., and Dowell E.L. Reduced–order models of unsteady viscous flows in turbomachinery using viscous-inviscid coupling. *Journal of Fluids and Structures*, 15:255–273, 2001.

Fage A. Experiments on a sphere at critical Reynolds numbers. Technical Report 1766, Aero. Res. Council, R and M, London, 1936.

Fournier G., Golanski F., and Pollard A. A novel outflow boundary condition for incompressible laminar wall-bounded flows. *Journal of Computational Physics*, 227:7077–7082, 2008.

Frondelius T., Koivurova H., and Pramilay A. Interaction of an axially moving band and surrounding fluid by boundary layer theory. *Journal of Fluids and Structures*, 22:1047–1056, 2006.

Howarth L. The boundary layer in three-dimensional flow. Part I - Derivation of the equations for flow along a general curved surface. *Phil. Mag. Serie 7*, 42:239–243, 1951.

Kaplun S. *The role of coordinate systems in Boundary Layer Theory*. Ph.D. thesis, California Institute of Technology, 1954.

Karimipanah M.T. and Olsson E. Calculation of three-dimensional boundary layers on rotor blades using integral methods. *Journal of Turbomachinary*, 115:342–353, 1993.

Lakshminarayana B. *Fluid Dynamics and Heat Transfer of Turbomachinery*. Wiley and Sons, 1995. 17376.

Morgan F. *Riemannian Geometry*. Jones Bartlett Publishers, 1993.

Nicols J.A. and Vega J.M. Three-dimensional streaming flows driven by oscillatory boundary layers. *Fluid Dynamics Research*, 32:119–139, 2003.

Pai S. *Viscous Flow Theory*. van Nostrand Co, 1956.

Panaras A. Boundary-layer equations in generalized curvilinear coordinates. Technical Report Technical Memorandum 100003, NASA, http://ntrs.nasa.gov/archive/nasa/casi.ntrs.nasa.gov/, 1987.

PETSc-FEM. A general purpose, parallel, multi-physics FEM program, GNU General Public License, http://www.cimec.ceride.gov.ar/petscfem. 2008.

Pope S.B. *Turbulent flows*. Cambridge, 2 edition, 2003.

Prado R. Reformulation of the momentum theory applied to wind turbinnes. *Journal of Wind Engineering and Industrial Aerodynamics*, 58:277–292, 1995.

Reed H.L. and Lin R.S. Effect of curvature on stationary crossflow instability of a three-dimensional boundary layer. *AIAA Journal*, 31(9):1611–1617, 1993.

Sagaut P. *Large eddy simulation for incompressible flows*. Springer, Berlín, 2001.

Schetz J.A. Numerical solution of the boundary layer equations using the finite element method. In D.M. N., editor, *Advances in Finite Element Analysis in Fluid Dynamics*, volume 123. ASME, 1991.

Schlitchting H. and Gersten K. *Boundary Layer Theory*. Springer, 8 edition, 2004.

Smith M.S. *Principles and applications of tensor analysis*. Howard W. Sams, 1963.

Spurk J.H. *Fluid mechanics*. Springer-Verlag, Germany, 1997.

Squire L.C. The three-dimensional boundary layer equations and some power series solutions. Technical Report Rpt. R&M 2006, ARC, 1957.

Stock H. en transition prediction in three-dimensional boundary layers on inclined prolate spheroids. *AIAA Journal*, 44(1):108–118, 2006.

Storti M. A pseudo-spectral approach for the incompressible boundary layer equations with automatic normal scaling. In S. Idelsohn, E. Oate, and E. Dvorkin, editors, *Computational Mechanics. New trends and applications*, pages 1–33. CIMNE, Barcelona, Spain, 1998.

Storti M.A. and D'Elía J. Added mass of an oscillating hemisphere at very-low and very-high frequencies. *ASME, Journal of Fluids Engineering*, 126(6):1048–1053, 2004.

White F.M. *Viscous Fluid Flow*. McGraw-Hill, New York, 3rd edition, 2005.

Wilcox D.C. *Turbulence Modeling for CFD*. DCW, 2nd edition, 1998.